

DMI Influence on the Integration, Leakage, and Threshold Property of Domain Wall Based Neurons

*Original*

DMI Influence on the Integration, Leakage, and Threshold Property of Domain Wall Based Neurons / Gaggio, Enrico; Graziano, Mariagrazia; Riente, Fabrizio. - In: IEEE TRANSACTIONS ON ELECTRON DEVICES. - ISSN 0018-9383. - 71:4(2024), pp. 2696-2701. [10.1109/TED.2024.3361849]

*Availability:*

This version is available at: 11583/2997533 since: 2025-02-16T10:46:57Z

*Publisher:*

Institute of Electrical and Electronics Engineers

*Published*

DOI:10.1109/TED.2024.3361849

*Terms of use:*

This article is made available under terms and conditions as specified in the corresponding bibliographic description in the repository

*Publisher copyright*

(Article begins on next page)

# DMI Influence on the Integration, Leakage, and Threshold Property of Domain Wall Based Neurons

Enrico Gaggio<sup>1</sup>, Mariagrazia Graziano<sup>1</sup>, and Fabrizio Riente<sup>1</sup>, *Member, IEEE*

**Abstract**—Interest in spintronic devices based on the motion of domain walls (DWs) has been growing rapidly as they are seen as potential components of neuromorphic information processing systems. In this article, we propose a leaky integrate-and-fire (LIF) neuron based on DW motion through spin orbit torque (SOT), in which the intrinsic leaking is achieved, thanks to the realization of an anisotropy gradient along the track. In particular, we studied the influence of Dzyaloshinskii–Moriya interaction (DMI) on the property of the neuron, showing how it affects the integration and leaking property of this type of structure. Moreover, we show how it offers a way to tune the leakage velocity of the DW, demonstrating how important DMI is in this kind of structure, showing that it plays a key role in regulating the SOT efficiency and the leaking speed. In addition, we exploited the voltage-controlled magnetic anisotropy (VCMA) effect to implement the neuron threshold. Finally, we show how all these ingredients can be combined together into a single device.

**Index Terms**—Artificial neuron, domain wall (DW), leaky integrate-and-fire (LIF) neuron, magnetic tunnel junction (MTJ), neuromorphic computing, voltage-controlled magnetic anisotropy (VCMA).

## I. INTRODUCTION

VON Neumann computing systems are able to tackle complex problems when given a structured set of data. On the other hand, the human brain is more proficient than Von Neumann computers when it comes to dealing with unstructured information from the environment. In fact, the human brain is able to solve certain problems more effectively than computers. Neuroscientists believe that this computational efficiency is due to intricate interactions between neurons and synapses. Neurons can be likened to a tree with dendrites, an axon, and a soma or cell body. The dendrites are where the neuron receives electrical impulses. The axon is the output structure of the neuron and sends electrical signals when

Manuscript received 13 August 2023; revised 22 December 2023; accepted 30 January 2024. Date of publication 9 February 2024; date of current version 26 March 2024. The review of this article was arranged by Editor B. Iñiguez. (Corresponding author: Fabrizio Riente.)

The authors are with the Electronics and Telecommunications Department, Politecnico di Torino, 10129 Torino, Italy (e-mail: fabrizio.riente@polito.it).

Color versions of one or more figures in this article are available at <https://doi.org/10.1109/TED.2024.3361849>.

Digital Object Identifier 10.1109/TED.2024.3361849

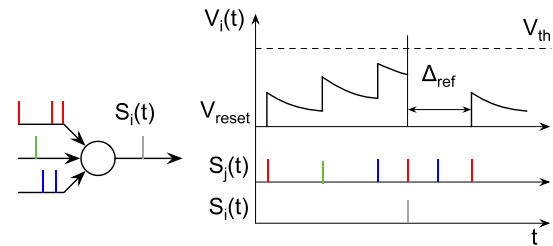


Fig. 1. LIF neuron working principle.

enough spikes have reached the neuron's input. Synapses provide electrical connections between the axon of one neuron and the dendrites of other neurons. One of the most popular models used to describe the working principle of the neuron is the so-called leaky integrate-and-fire (LIF) neuron [1]. The LIF neuron principle is depicted in Fig. 1 and it can be summarized by three main features [2].

- 1) Integration: the LIF neuron integrates the incoming signals summing up the spikes coming from its synaptic inputs. This signal is accumulated in a quantity called membrane potential, which deflects from its resting value.
- 2) Leaking: if no input arrives to the neuron, the membrane potential naturally drops toward its resting value.
- 3) Firing: when the membrane potential reaches a threshold value, the neuron emits an output spike.

Due to the higher energy efficiency of brain computation with respect to standard computers [3], in the past years researchers put a lot of effort in developing systems inspired by the functionality of neuron and synapsis. This field is called neuromorphic computing. Among the proposals that can be found in the literature, there are solutions based on transistors and CMOS systems [4], [5], and others based on nonvolatile devices such as memoristors [6] and spintronic systems [7], [8]. Spintronic systems are usually based on domain wall (DW) motion in the free layer of a magnetic tunnel junction (MTJ). For these kinds of devices, one of the trickiest features to achieve and control is intrinsic leaking of the neuron. To obtain this characteristic in a DW-based neuron (i.e., the natural drift of the DW toward its resting position), researchers proposed several solutions, such as shape-based anisotropy, dipolar field coupling, and anisotropy gradient [7], [9], [10].

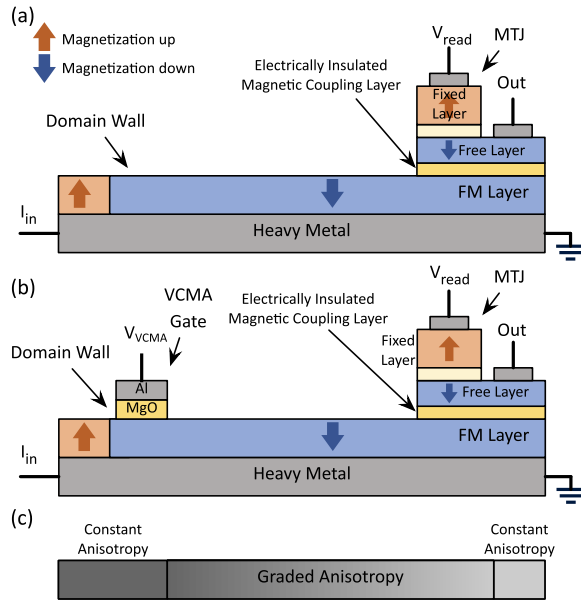


Fig. 2. (a) Device structure. (b) Device structure including the VCMA gate. (c) Schematic representation of the simulated structure to introduce leaking, dimensions are not to scale.

The contribution of the work can be listed as follows: 1) we propose an MTJ neuron based on DW motion in which the intrinsic leaking is achieved with a graded anisotropy track, where the current-induced spin orbit torque (SOT) is exploited; 2) we perform an in-depth analysis on the influence of the Dzyaloshinskii–Moriya interaction (DMI) on all the properties of the neuron; and 3) we study the possibility of exploiting the voltage control magnetic anisotropy (VCMA) effect to implement a current threshold for the neuron. Concerning the DMI, we demonstrate how it affects the integration and leaking properties of the structure and how this parameter can be exploited to tune the leakage velocity of the neuron. In fact, there are experimental studies that showed how the DMI coefficient can be tuned by playing with the heterostructure property, e.g., working on the thickness of the heavy metal (HM) [11] or adding a wedge of *Pt* between the FM and the oxide layer [12]. Moreover, we investigated the influence of the DMI on the efficiency of the VCMA gate barrier. Finally, we combined all these features into a single device.

## II. DEVICE STRUCTURE

The basic structure of the proposed device is reported in Fig. 2(a). It is a four-terminal device composed of two main elements: a racetrack in which the DW moves and an MTJ. These two elements are electrically insulated one from the other, thanks to an electrically insulated magnetic coupling layer. The structure is similar to the one proposed in [13], but in this case input current pulses are injected into the HM layer placed below the ferromagnet, to achieve the motion of the DW toward the MTJ through the SOT mechanism. When the DW reaches the portion of the racetrack below the MTJ, thanks the magnetic coupling, the magnetization in the free layer of the MTJ switches, bringing the MTJ in its low resistance state. If a reading voltage is applied to the MTJ, this change in its resistance state leads to the emission of an

TABLE I  
PARAMETERS USED IN ALL THE SIMULATIONS

Parameter	Value
Ferromagnetic Layer Width	40 nm, 100 nm
Ferromagnetic Layer Thickness	1 nm
Heavy Metal (HM) Thickness	1 nm
Saturation Magnetization, $M_{sat}$	$10^6 \frac{A}{m}$
Exchange Stiffness Interaction, $A_{ex}$	$1 \times 10^{-11} \frac{J}{m}$
Anisotropy Constant, $K_{u1}$	$0.8 \times 10^6 \frac{J}{m^3}$
Damping Factor, $\alpha$	0.02
Non-Adiabatic parameter, $X_i$	0.2
$\mu_0$	$4\pi \times 10^{-7} \frac{H}{m}$
DMI coefficient	0.1, 0.2, 0.3, 0.6 $\frac{mJ}{m^2}$
T	0 K
$\hbar$	$1.0545718 \times 10^{-34} J\cdot s$
e	$1.6021766 \times 10^{-19} C$
$\alpha_{H,DL}$	0.15
Landè Factor	2

output current by the device. The leaking behavior is achieved by creating a track in which the anisotropy gradually varies between two extreme values [Fig. 2(c)]. The anisotropy can be varied by irradiating the track with a focus ion beam with  $Ga^+$  ions, as has been experimentally proven in [14]. In addition, we added a gate to the structure exploiting the voltage-controlled magnetic anisotropy (VCMA) effect to create an energy barrier for the DW [Fig. 2(b)]. The voltage applied to a gate placed above a ferromagnetic material locally modifies the magnetic anisotropy in the region below the gate [15], where the anisotropy is constant. The anisotropy variation is proportional to the voltage applied. The VCMA effect can be used to implement a current threshold for the neuron: the DW can overcome the barrier only if a current spike with an amplitude high enough is injected into the HM layer. For example, this threshold could be used to inhibit some neurons with respect to others in a hypothetical performance of a network.

## III. METHODOLOGY

The racetrack in which the DW moves has been simulated with the Mumax3 micromagnetic simulator [16]. All the details about the simulated structure are presented in Section IV. The analysis has been divided into two main stages.

- 1) Stage I: first, in Section IV-B, the possibility of using the VCMA to implement a current threshold for the neuron and the dependence of the efficiency of the barrier with respect to the value of DMI coefficient is studied. Then, the leaking due to the anisotropy gradient and the dependence of the drift of the DW on the strength of the DMI interaction is studied in detail (Section IV-C).
- 2) Stage II: here, the response of the DW to current spike trains of different frequencies is shown. Depending on the working frequency, one can tune the leaking relaxation velocity selecting a suitable value for the DMI coefficient.

## IV. SIMULATIONS AND RESULTS

The simulation parameters used for the analysis and characterization of the proposed device are reported in Table I and

taken from [17]. The HM layer and the ferromagnetic layer are both 1-nm thick. We considered two different racetrack widths, 40 and 100 nm. The track was discretized with cells of  $1 \times 1 \times 1 \text{ nm}^3$ . The exchange stiffness  $A_{\text{ex}}$  is  $1.0 \times 10^{-11} \text{ J/m}$ , the Landau–Lifshitz–Gilbert damping constant  $\alpha$  is 0.02, the nonadiabaticity factor  $\chi_i$  is 0.2, and the magnetic saturation  $M_{\text{sat}}$  is  $0.8 \times 10^6 \text{ A/m}$ . To study the effect of DMI in the movement of DW, four different values of the DMI coefficient have been analyzed: 0.1, 0.2, 0.3, and 0.5 ( $\text{mJ/m}^2$ ). When needed, the SOT arising due to the current flowing in the HM layer is modeled through the definition of two custom fields. The DW is a Néel-type. Other details about the simulations, peculiar of a specific analysis, will be provided in the relative sections or can be found in the additional information on Zenodo [18].

### A. Stage I: Integration

The first characteristic studied is the integration property of the device as a function of the DMI coefficient for the two different widths of the racetrack. To perform this study, the DW is initiated at the beginning of the track and we provided as input three current pulses, with amplitude  $3 \times 10^{10}$ ,  $7.5 \times 10^{10}$ , and  $5 \times 10^{10} \text{ A/m}^2$ , respectively. Each spike lasts for 2.5 ns and the time between them is 20 ns. The results for the two widths of the racetrack are reported in Fig. 3. Note that at this stage no leaking feature was yet implemented, so when the current is turned off the DW reaches a stable position in the track and stays there. Looking at Fig. 3(a) and (b), it can be observed how DMI strongly influences DW motion: for low values of the DMI coefficient, the efficiency of the SOT mechanism is decreased and, for the same current spike, the DW travels for a shorter distance. Moreover, the time required for the DW to reach a stable position increases. For the racetrack of width 40 nm, the results obtained are much more similar. It appears that thinner tracks allow to partially compensate the loss of efficiency due to the decrease in the DMI coefficient.

### B. Stage I: VCMA Threshold Effect

In this section, the influence of DMI and width of the track on the VCMA barrier is analyzed. The gate considered in the simulation is 40-nm large and its width is equal to the one of the racetrack. It is defined as a region with an anisotropy value +1%, +3%, or +5% higher than the value of the magnetic anisotropy in the other portion of the track. The gate center is placed at  $-55 \text{ nm}$ . The DW is stimulated with current pulses 2.5-ns wide, of increasing intensity; the time between two spikes is 1.0 ns and the amplitude is increased by  $0.10 \text{ A/m}^2$  each time. It was decided to increase the current with such a small step to better identify the threshold current. The work presented in [19] already showed the possibility of creating a barrier for the DW exploiting the VCMA effect. Indeed, when a voltage is applied to the VCMA gate, the consequent anisotropy variation creates a barrier for the DW, which can be overcome only if the current responsible for DW motion is above a certain threshold. This threshold depends on the voltage applied to the gate, since it

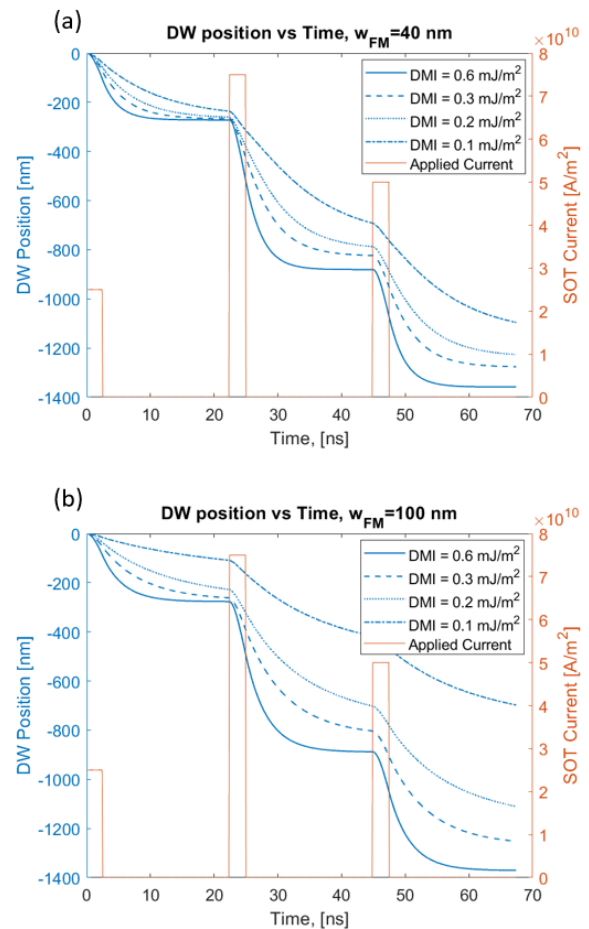


Fig. 3. DW response to current pulses of different amplitudes and values of the DMI coefficient. (a) Results for the racetrack whose width is 40 nm. (b) Ones for the 100-nm track. Note that no leaking feature was yet implemented.

regulates the amount of anisotropy variation. Here we focused on the influence of the DMI coefficient and the width of the track on barrier effectiveness. In Fig. 4 are reported the results obtained for the different values of the considered DMI coefficient. In particular, Fig. 4(a) and (b) shows the DW motion along the 40-nm-wide track for anisotropy variation of +1% and +5%, respectively. Fig. 4(c) reports the results for the 100-nm-wide track with an anisotropy variation of +5%. The first thing that can be noted is that the current threshold is higher for higher values of anisotropy variation below the VCMA gate and it tends to increase if the DMI coefficient is reduced. This is in agreement with several studies [20], [21], which proved that the DMI plays a crucial role in the efficiency of the SOT mechanism. Therefore, if the DMI coefficient is reduced, a higher current is needed to provide enough energy to the DW to make it overcome the barrier. Moreover, in the 100-nm-wide racetrack for values of the DMI coefficient equal to 0.1 and 0.2  $\text{mJ/m}^2$  (the lowest considered in this study), even if the DW is able to overcome the barrier, its motion becomes unstable especially for high current values. This is particularly true for the case where the DMI is 0.1  $\text{mJ/m}^2$ , where the DW even if it manages to overcome the barrier has an unstable motion and a very low speed even if the current increases.

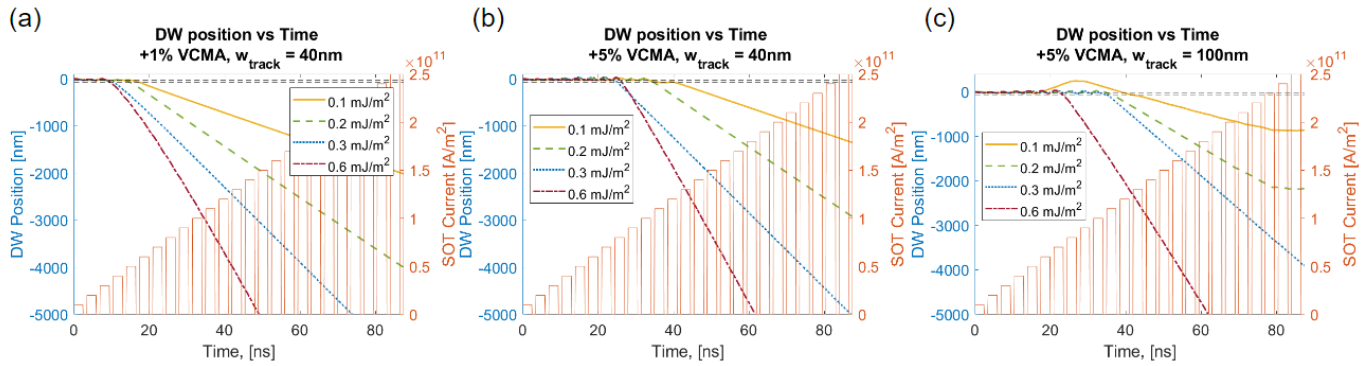


Fig. 4. Effect of the VCMA barrier on the DW motion for different values of the DMI coefficient. Results for (a) and (b) 40-nm-wide racetrack and (c) 100-nm-wide track.

These instability of the DW trajectory, for the 100-nm-wide track, was also observed when the anisotropy variations were +1% and +3%. This does not happen for the 40-nm track, in which the DW is able to overcome the barrier and it has a stable motion also for the other anisotropy variation considered even if the DMI is reduced. In general, in the narrower track we observed a more stable DW motion and better functionality of the VCMA gate.

### C. Stage I: Leaking

To achieve an intrinsic leaking of the neuron, the motion of a DW in a racetrack with a graded anisotropy has been studied for different values of the DMI coefficient. Indeed, when there is a gradient in the anisotropy along the track and no current stimuli are applied, the DW tends naturally to move toward the region with lower anisotropy, since it represents a more energetically favorable configuration. The simulated racetrack, whose total length is 850 nm, is constituted by two larger regions of 25 nm, one at the beginning and the other at the end of the track, in which the anisotropy is fixed at  $K_{u,\min} = 0.8 \times 10^6 \text{ J/m}^3$  and  $K_{u,\max} = 1.6 \times 10^6 \text{ J/m}^3$ , respectively. These two values correspond to the extreme values of the magnetic anisotropy. To achieve a gradual variation in anisotropy between these two regions, the anisotropy is varied each 10 nm, by an amount  $\Delta$  defined as follows:

$$\Delta = \frac{K_{u,\max} - K_{u,\min}}{N_{\text{reg}}}$$

where  $N_{\text{reg}} = 80$  corresponds to the number of regions of 10 nm in between the two extreme regions. The result is step-like graded anisotropy profile, similar to what can be practically obtained in a fabrication process. The DW is initialized at  $\approx 825 \text{ nm}$ , closer to the high anisotropy region of the track and the simulation is performed letting the system to relax without any stimuli applied. This has been done for track's widths equal to 40 and 100 nm, and for values of the DMI coefficient of 0.05, 0.1, 0.2, and 0.3 mJ/m².

The results for the 40- and 100-nm racetrack are reported in Fig. 5(a) and (b), respectively. It can be seen that in both the cases, the strength of the DMI highly influences the drift of the DW: the time required by the DW to reach the

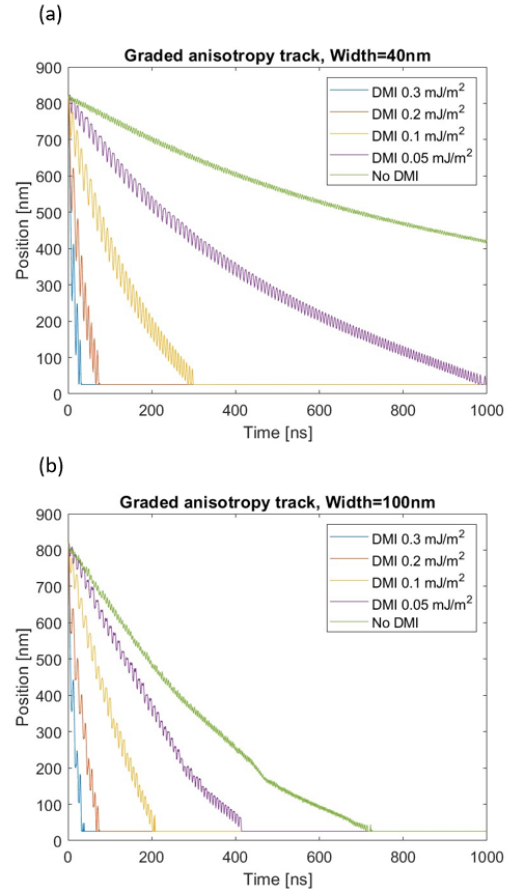


Fig. 5. Drift of the DW in the racetrack due to the anisotropy gradient for different values of DMI coefficient. Results for (a) 40-nm-wide racetrack and (b) 100-nm-wide racetrack.

TABLE II  
RELAXATION TIME AND RELAXATION VELOCITIES  
ESTIMATION FOR THE 40-NM-WIDE TRACK

Quantity	0.05 $\frac{\text{mJ}}{\text{m}^2}$	0.1 $\frac{\text{mJ}}{\text{m}^2}$	0.2 $\frac{\text{mJ}}{\text{m}^2}$	0.3 $\frac{\text{mJ}}{\text{m}^2}$
Relax. Time [ns]	980	287	67	26
Relax. Velocity [nm/ns]	-0.81	-2.79	-11.9	-30.7

lower anisotropy end of the track reduces considerably as the DMI coefficient is increased. A more detailed information about this characteristic is provided by the data summarized in Tables II and III, where the relaxation times (i.e., the time

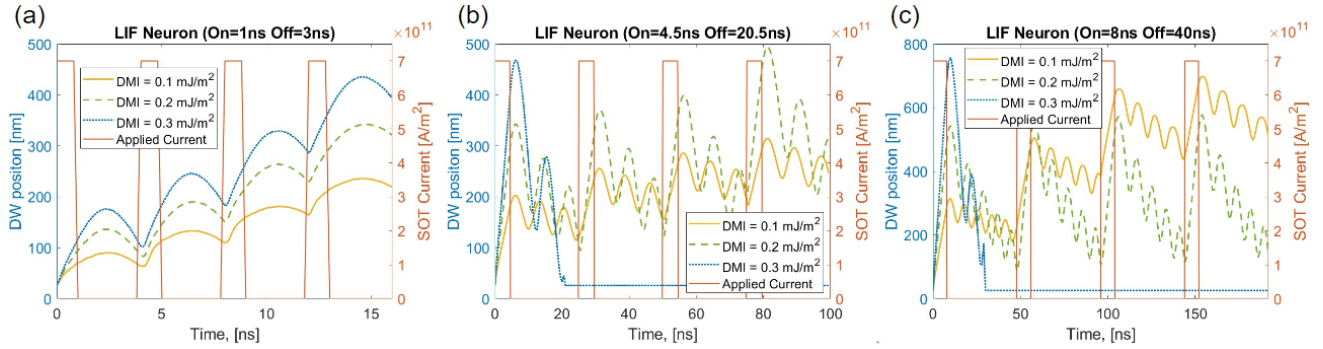


Fig. 6. Response of the DW-based neuron to current pulses for different values of DMI coefficient. The on time of the spikes and the frequency is different in the three graphs. (a) On time 1 ns, (b) on time 4.5 ns, and (c) 8 ns.

TABLE III

RELAXATION TIME AND RELAXATION VELOCITIES  
ESTIMATION FOR THE 100-NM-WIDE TRACK

Quantity	0.05 $\frac{\text{mJ}}{\text{m}^2}$	0.1 $\frac{\text{mJ}}{\text{m}^2}$	0.2 $\frac{\text{mJ}}{\text{m}^2}$	0.3 $\frac{\text{mJ}}{\text{m}^2}$
Relax. Time [ns]	415	202	68	32
Relax. Velocity [nm/ns]	-1.92	-3.94	-11.8	-24.9

required by the DW to reach the other end of the track) and the relaxation velocities for the different values of the DMI coefficient considered are reported. The oscillatory behavior of the DW during leaking is due to oscillations in the evolution of the DW total energy, whose main contributions are the anisotropy and demagnetization energies. Since not in all the cases the trajectory of the DW could be approximated with a straight line, the relaxation velocity has been estimated taking the average of the vector of the instantaneous velocity (computed as  $\Delta x / \Delta t$ , where  $\Delta x$  is the shift in the DW position in the simulation sample time  $\Delta t$ ). When the DMI is low, the drift of the DW is much faster in the 100-nm-wide racetrack. In particular, for a DMI coefficient of 0.05  $\text{mJ}/\text{m}^2$ , the time required by the DW to reach the other end of the track is 980 ns for the 40-nm-wide track and 415 ns for the 100-nm-wide one. This difference in relaxation times decreases if the DW coefficient is 0.1  $\text{mJ}/\text{m}^2$  but in the 100-nm racetrack still the DW moves faster; the trend changes if the DMI coefficient is further increased, in that case the DW drift is slightly faster in the narrower track.

The analysis performed has shown that the natural drift of the DW toward the lower anisotropy region of the track, thanks to the gradient in the anisotropy, is highly influenced by the strength of the DMI. Therefore, the DMI coefficient offers a possibility to tune the relaxation time of the neuron. This can be taken into account while designing the structure of the network: if one plans to work with a certain frequency of the input current pulses, the neurons could be designed to have a proper value of DMI coefficient, selecting the most suitable value of relaxation time.

#### D. Stage II: Device Response to Current Pulses

In this section, the response of the DW to pulses of different frequencies and different time duration is explored, for three different values of DMI coefficient (0.1, 0.2, and 0.3  $\text{mJ}/\text{m}^2$ ). The pulses have all the same amplitude,  $7 \times 10^{11} \text{ A}/\text{m}^2$ , and the racetrack in which the DW moves is the graded anisotropy track studied in Section IV-C.

In Fig. 6(a) are reported the results when the input is a train of four pulses with an on and off times of 1 and 3 ns, respectively. For all the three values of DMI coefficient considered, the DW moves as expected: when the current pulse is on, the DW moves further in the track; on the contrary, when the current is off, its start to drift back, thanks to the anisotropy gradient. Coherently with the results reported in Section IV-C, the greater the DMI coefficient, the faster the leaking. At the same time, if the DMI is increased, the DW travels for a longer distance when the current is on, since the efficiency of the SOT is increased. After the fourth current spike, the farthest DW's position is obtained for a DMI coefficient equal to 0.3  $\text{mJ}/\text{m}^2$ . In Fig. 6(b) are presented the results obtained when the on time of the pulses is 4.5 ns and the time between two spikes is 20.5 ns. The general behavior is the same as the previous set of pulses, but in this case, for DMI equal to 0.3  $\text{mJ}/\text{m}^2$ , the leaking of the DW is so fast that during the off time the DW is able to drift back to its initial position. In this case, after the fourth pulse, the further DW's position on the track is reached when the DMI coefficient is equal to 0.2  $\text{mJ}/\text{m}^2$ . Finally, in Fig. 6(c) are reported the results for  $t_{\text{on}} = 8$  ns and  $t_{\text{off}} = 40$  ns. In this case, the time between two pulses is big enough to let the DW relax to its initial position also when the DMI coefficient is 0.2  $\text{mJ}/\text{m}^2$ . For a DMI coefficient of 0.1  $\text{mJ}/\text{m}^2$ , the DW response is the correct one: even if the leaking is present, after each pulse the DW reaches a position that is further than the one achieved after the previous pulse. These simulations have shown how the DMI coefficient is an important parameter to consider when designing an LIF-neuron based on DW motion through SOT in a graded anisotropy track, since it plays a key role in regulating the SOT efficiency and the leaking speed. In particular, if one plans to work with current pulses of short time duration and high frequency, higher values of DMI coefficient can be considered [Fig. 6(a)]; on the other hand, if the width in time of the pulses is increased and the frequency is reduced, the DMI coefficient must be reduced to avoid the drift of the DW to its initial position in the time between two current spikes [Fig. 6(c)].

#### E. Stage II: Device With the VCMA Gate

For completeness, in this final part all the features of the neuron analyzed in the Stage I are put together to study the behavior of the DW when both the leaking and the VCMA gate are implemented. The leaking is obtained using the 40-nm

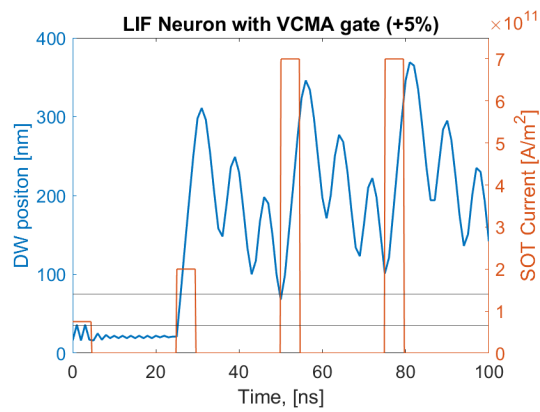


Fig. 7. LIF neuron based on the 850-nm graded anisotropy track racetrack with the VCMA gate.

racetrack with a graded anisotropy described in Section IV-C. The width of the VCMA gate is 40 nm and its center is placed at 55 nm. Since the gate is placed adjacent to the region with the minimum anisotropy, the anisotropy variation in the region below the gate is set to be +5% of the minimum anisotropy value (i.e.,  $0.8 \times 10^6 \text{ J/m}^3$ ). The value of DMI coefficient considered is  $0.2 \text{ mJ/m}^2$  and the DW is stimulated with four current pulses of different amplitude; their time duration is equal to 4.5 ns and occur each 20.5 ns. The result is reported in Fig. 7. The first current pulse, whose amplitude is  $0.75 \text{ A/m}^2$ , is not sufficient to provide enough energy to the DW to overcome the VCMA barrier. This is in accordance with the results obtained in Section IV-B, which has shown that for a DMI coefficient of  $0.2 \text{ mJ/m}^2$  and a VCMA variation of +5%, the threshold current for the DW is  $\approx 1.0 \text{ A/m}^2$ . With the second pulse, whose amplitude is  $2.0 \text{ A/m}^2$ , the DW is able to overcome the VCMA barrier. Then, the device behaves exactly as expected: when the current is off, the DW drifts toward its initial position, implementing the leaking functionality; instead, when the current is on, it moves further along the track getting closer to the hypothetical position of the MTJ.

## V. CONCLUSION

We proposed an LIF neuron based on DW motion through SOT, in which the leaking feature was obtained, thanks to the realization of an anisotropy gradient along the track. Moreover, the possibility of exploiting the VCMA effect to implement a current threshold for the neuron was studied. A lot of effort was dedicated to study the influence of the DMI on all the features of the neuron, proving that it plays a key role in the efficiency of DW motion, in the effectiveness of the VCMA gate, and in the leaking time of the DW. This study suggests that during the design of LIF neurons, particular care should be taken to tune the right DMI coefficient during the fabrication process. However, this preliminary work is a starting point for further investigations, intending to take into account the effect of edge roughness and thermal noise into the proposed device.

## REFERENCES

- [1] E. Hunsberger and C. Eliasmith, "Spiking deep networks with LIF neurons," 2015, *arXiv:1510.08829*.
- [2] W. Gerstner, W. M. Kistler, R. Naud, and L. Paninski, *Neuronal Dynamics: From Single Neurons To Networks and Models of Cognition*. Cambridge, U.K.: Cambridge Univ. Press, 2014.
- [3] A. Mehonic and A. J. Kenyon, "Brain-inspired computing needs a master plan," *Nature*, vol. 604, no. 7905, pp. 255–260, Apr. 2022.
- [4] M. A. Khanday, F. A. Khanday, and F. Bashir, "Single SiGe transistor based energy-efficient leaky integrate-and-fire neuron for neuromorphic computing," *Neural Process. Lett.*, vol. 55, no. 6, pp. 6997–7007, Dec. 2023.
- [5] R. Cao et al., "Compact artificial neuron based on anti-ferroelectric transistor," *Nature Commun.*, vol. 13, no. 1, p. 7018, Nov. 2022.
- [6] J.-Q. Yang et al., "Leaky integrate-and-fire neurons based on perovskite memristor for spiking neural networks," *Nano Energy*, vol. 74, Aug. 2020, Art. no. 104828. [Online]. Available: <https://www.sciencedirect.com/science/article/pii/S2211285520303852>
- [7] W. H. Brigner et al., "Shape-based magnetic domain wall drift for an artificial spintronic leaky integrate-and-fire neuron," *IEEE Trans. Electron Devices*, vol. 66, no. 11, pp. 4970–4975, Nov. 2019.
- [8] W. A. Misba, T. Kaisar, D. Bhattacharya, and J. Atulasimha, "Voltage-controlled energy-efficient domain wall synapses with stochastic distribution of quantized weights in the presence of thermal noise and edge roughness," *IEEE Trans. Electron Devices*, vol. 69, no. 4, pp. 1658–1666, Apr. 2022.
- [9] W. H. Brigner et al., "Three artificial spintronic leaky integrate-and-fire neurons," in *SPIN*, vol. 10, no. 2. Singapore: World Scientific, 2020, p. 2040003.
- [10] W. H. Brigner et al., "Graded-anisotropy-induced magnetic domain wall drift for an artificial spintronic leaky integrate-and-fire neuron," *IEEE J. Explor. Solid-State Comput. Devices Circuits*, vol. 5, no. 1, pp. 19–24, Jun. 2019.
- [11] J. Torrejon et al., "Interface control of the magnetic chirality in CoFeB/MgO heterostructures with heavy-metal underlayers," *Nature Commun.*, vol. 5, no. 1, p. 4655, Aug. 2014.
- [12] X. Ma et al., "Interfacial control of Dzyaloshinskii–Moriya interaction in heavy metal/ferromagnetic metal thin film heterostructures," *Phys. Rev. B, Condens. Matter*, vol. 94, no. 18, Nov. 2016, Art. no. 180408.
- [13] W. H. Brigner et al., "CMOS-free multilayer perceptron enabled by four-terminal MTJ device," 2020, *arXiv:2002.00862*.
- [14] D. Giuliano et al., " $\text{Ga}^+$  ion irradiation-induced tuning of artificial pinning sites to control domain wall motion," *ACS Appl. Electron. Mater.*, vol. 5, no. 2, pp. 985–993, Feb. 2023.
- [15] T. Nozaki et al., "Recent progress in the voltage-controlled magnetic anisotropy effect and the challenges faced in developing voltage-torque MRAM," *Micromachines*, vol. 10, no. 5, p. 327, May 2019.
- [16] A. Vansteenkiste, J. Leliaert, M. Dvornik, M. Helsen, F. Garcia-Sanchez, and B. van Waeyenberge, "The design and verification of MuMax3," *AIP Adv.*, vol. 4, no. 10, Oct. 2014, Art. no. 107133.
- [17] R. Tomasello, E. Martinez, R. Zivieri, L. Torres, M. Carpentieri, and G. Finocchio, "A strategy for the design of skyrmion racetrack memories," *Sci. Rep.*, vol. 4, no. 1, pp. 1–7, Oct. 2014.
- [18] E. Gaggio, M. Graziano, and R. Fabrizio, Dec. 2023, "vlsi-nanocomputing/leaky-integrate-and-fire-neuron: Version-1.0.0," *Zenodo*, doi: [10.5281/zenodo.10308176](https://doi.org/10.5281/zenodo.10308176).
- [19] P. Diona, L. Gnoli, and F. Riente, "Simulation and modeling of racetrack memories with VCMA synchronization," *IEEE Trans. Electron Devices*, vol. 69, no. 7, pp. 3675–3680, Jul. 2022.
- [20] Y. Quessab, J. Xu, M. G. Morshed, A. W. Ghosh, and A. D. Kent, "Interplay between spin-orbit torques and Dzyaloshinskii–Moriya interactions in ferrimagnetic amorphous alloys," *Adv. Sci.*, vol. 8, no. 18, Sep. 2021, Art. no. 2100481.
- [21] J. Yu et al., "Spin orbit torques and Dzyaloshinskii–Moriya interaction in dual-interfaced Co-Ni multilayers," *Sci. Rep.*, vol. 6, no. 1, p. 32629, Sep. 2016.